COMMUNICATIONS IN SCIENCE AND TECHNOLOGY
Homepage: cst.kipmi.or.id

Biochar supported photocatalyst (mangrove biochar-TiO_2) for organic pollutants removal via synergetic adsorption-photocatalytic process

Nadya Ummi Azizah[a,c], Dessy Ariyanti[a,b,c,*], Dina Lesdantina[a,b,c], Erwan Adi Saputra[d], Vimal Chandra Srivastava[e]

[a]*Department of Chemical Engineering, Faculty of Engineering, Universitas Diponegoro, Semarang 50275, Indonesia*
[b]*SDGs Center, Universitas Diponegoro, Semarang 50275, Indonesia*
[c]*Center of Advanced Materials for Sustainability, Universitas Diponegoro, Semarang 50275, Indonesia*
[d]*Department of Chemical Engineering, Faculty of Engineering, Universitas Pembangunan Nasional "Veteran", Surabaya 61119, Indonesia*
[e]*Department of Chemical Engineering, Indian Institute of Technology Roorkee, Roorkee, Uttarakhand 247667, India*

Article history:
Received: 18 December 2024 / Received in revised form: 19 June 2025 / Accepted: 22 June 2025

Abstract

Access to clean water remains a global challenge, which is made worse by the contamination of chemical dyes. The recent innovations of wastewater treatment have been introduced, such as combined biochar with TiO_2 photocatalyst. This study proposed to degrade mainly organic pollutants from dyed wastewater using adsorption-photocatalytic of biochar-supported photocatalyst TiO_2 (BSP). Mangroves were converted into biochar via hydrothermal carbonization process and combined with TiO_2 by a sol-gel method. The composite was then characterized by SEM-EDX, FTIR, and XRD. The degradation performance of the BSPs was optimized with the addition of Titanium (IV) Isopropoxide (TTIP) solution in biochar for 15-25 mL, solution photocatalyst dosage 0.5–1 g/L, initial dyed water concentration at 10 ppm, pH 5.2, and UV-irradiation time from 30 to 240 min in a photocatalytic reactor. The phenomenon of organic pollutants removal was observed based upon the mechanism and dominance of the process and the degradation reaction rate of organic pollutants in dyed wastewater. Methylene blue used as a model dye was degraded 100% through the adsorption-photocatalysis process using BSP. The highest effective degradation performance was found in BSP 20 that had a functional group area of 4.39923 m^2/g, a catalyst loading of 0.5 g/L, and the highest degradation rate at k = 0.021 min^{-1}. In subsequent development, the synergistic interaction between biochar and TiO_2 presents a promising avenue for the development of advanced wastewater treatment systems targeting the removal of organic pollutants, particularly in textile industry.

Keywords: Mangrove biochar; adsorption-photocatalysis synergy; titanium dioxide; wastewater treatment

1. Introduction

Global water demand is growing inversely the accessibility of drinkable water for humans. As reported by World Wildlife Foundation, about one billion people worldwide struggle to access clean water [1]. Some studies reported that worldwide wastewater, including dyed wastewater, reaches nearly 380 billion cubic meters per year [2]. Wastewater generated by textile industries is characterized by dark color, high concentrations of aromatic pollutants, alkaline properties, and complex substances [3]. It is estimated that more than 10 – 40% of chemically reactive dyes are wasted during the textile manufacturing process [4], which poses potential risks to humans and other organisms.

Extensive treatment is deemed critical to be applied to wastewater and azo dyes to achieve environmental quality standards. Various technologies [5,6] such as ozone oxidation, ultrafiltration, adsorption, photocatalysis, coagulation, and flocculation have been applied to remove these organic pollutants. Adsorption and photocatalysis, in this case, have been widely utilized in wastewater treatment; however, both have their distinctive challenges. Producing adsorbents such as activated carbon, zeolite, alumina, and silica is high-priced, thus encouraging the development of other economical alternative adsorbents such as biochar.

Biochar is a carbon-rich substance that has a broad superficial area and functional groups, high porosity [7], and aloft relative carbon content of 40-75% [8-9]. It can be produced from the thermal conversion process of animal and plant biomass [10], such as seaweed [11], waste ginkgo leaf [12], waste walnut shell [13], and palm kernel shell [14]. So far, there are only a few studies on biochar from mangrove plants. Most of the C elements in mangroves are stored in the roots (37.03 – 40.89%), leaves (34.25 – 41.74%) [15], and twigs (42.40 – 43.05%) [16]. The organic carbon content in living mangrove roots (33.87 ± 1.98%) is marginally greater than that of the dead ones (32.65 ± 1.28%) [17].

* Corresponding author.
Email: dessy.ariyanti@che.undip.ac.id
https://doi.org/10.21924/cst.10.1.2025.1619

In many cases, TiO_2 photocatalyst is also used due to its excellent ability to break down organic pollutants through the photocatalysis process [18]. However, because of its wide band gap (Eg = 3.2 eV), TiO_2 is only activated using UV or near-UV light [19]. To improve its photocatalytic performance, TiO_2 can be combined with biochar as biochar-supported photocatalysts (BSP) [20] that may (i) enhanced photocatalytic performance compared to pure TiO_2; (ii) have a large and efficient electron storage capacity that supplies electrons to TiO_2, and (iii) added C–O–Ti linkages within the composite structure that reduces the semiconducting energy gap and broadens the adsorption range to decrease energy levels [21]. A recent study by Ulfa et al. [22] explored various supports for TiO_2 by synthesizing TiO_2-impregnated mesoporous silica using a gelatin–P123 biotemplating method in which the results showed methylene blue (MB) degradation up to 95%. This suggests that combining TiO_2 with structurally tailored supports significantly can improve their performance.

In this research, mangrove biomass was converted into biochar through the hydrothermal carbonization (HTC) process at an optimal temperature of 250°C, as supported by previous studies on the efficiency for heat generation [13],[23–25]. Mangrove biochar was incorporated with TiO_2 through the sol-gel method. Other methods have also been applied by other researchers, such as Yue et al. [26], producing BSP from barley-straw using the ultrasound-assisted method to degrade methylene blue; Shi et al. [27] synthesizing a BSP using the hydrogenation method from sugarcane bagasse, and Martins et al. [21] converting paper into magnetic biochar to produce BSP through the solvothermal process for the degradation of Sulfadiazine (SDZ) and Oxolinic acid (OXA).

This study reported the synergetic effect of biochar and TiO_2 photocatalyst through adsorption-photocatalysis experiments and physicochemical characterization. The photodegradation was performed in the organic pollutant removal using methylene blue as a model dye solution under UV irradiation loaded with a fine BSP. The mechanism of both solids was proposed based on the kinetics of methylene blue degradation. This study also offers a theoretical encouragement for the synergistic interaction between mangrove biochar and TiO_2 in the decay of organic contaminants.

2. Materials and Methods

2.1. Materials preparation

The biomass used was derived from mangrove plants, particularly twigs and roots, which were obtained from Tapak Mangrove Tourism Village, Semarang. Furthermore, Titanium (IV) Isopropoxide (TTIP) was purchased from Qingdao CEMO Biotechnology Co., Ltd. TiO_2 was synthesized from TTIP via a sol-gel process and other chemicals such as Ethanol, HCl, and acetic acid were from Supelco Merck (Sigma-Aldrich).

2.2. Synthesis of biochar

Mangrove twigs and roots were grounded and filtered for a 100–150µm particle size range. Biochar was prepared by mixing 6.5 grams of biomass with 65 ml of distilled water (1:10wt%) in a 100 ml Teflon-linked Autoclave. The hydrothermal carbonization method was carried out at 250°C for 3 hours [28]. Afterward, the biochar was left for 24 hours at room temperature before being filtered off and washed using DI water. The initial pH of biochar was about 5.9 – 6.1. Using acid treatment, the biochar was later rinsed with HCl 0.1 M until the pH of the biochar dropped 1-2 levels to increase the functional groups [29]. It was then placed in a vacuum oven at 110°C for 2 hours.

2.3. Synthesis of biochar-supported photocatalyst

The sol-gel method was utilized to incorporate mangrove biochar with TiO_2. 5 grams of biochar was dispersed in 60 ml of ethanol and agitated for 2 hours [30]. TTIP at 15 ml, 20 ml, and 25 ml was dropped into each experimental container. After a 2 hour-stirring, 2.5 ml of deionized water and acetic acid was added by drop. The stirring continued for the next 2 hours until a gel was formed, which later on was left overnight. The solid obtained was transferred to a binder oven set at 105°C for 1 hour and calcined at 500°C for another hour to generate TiO_2 crystals.

2.4. Characterization

The surface morphology of the BSP was identified by means of scanning electron microscopy (SEM-EDX JEOL JSM-6510LA). The crystallinity of pure TiO_2, mangrove biochar, and BSP samples were analyzed by X-ray diffraction spectroscopy (XRD Bruker 8D Advance), scanned at 2θ=10°-80°. Fourier Transform Infrared Spectroscopy (FTIR Perkin-Elmer UATR Spectrum Two) was used to analyze the functional group on the biochar and BSPs and the data were also analyzed with the help of Origin software to obtain the functional group area of each sample. Furthermore, UV-visible spectrophotometry (Double Beam Spectrophotometer UH5300) was in use to evaluate the degradation performance.

2.5. Effectiveness of adsorption and photocatalysis

The effectiveness of the adsorption-photocatalytic activity of all BSPs was examined by the kinetics of methylene blue (MB) degradation. The initial volume for methylene blue was determined to be 500 mL with a concentration of 10 ppm. The concentration of MB at the beginning and fixed intervals of the process was measured by adsorption in a dark optical box and photocatalytic using UV-visible light irradiation. The methylene blue solution and BSP sample were then mixed and stirred in each experiment with a magnetic stirrer and various catalyst dosages (0.5, 0.75, and 1 g/L). The photocatalytic process was performed in a custom photocatalytic reactor incorporating a Philips UV sterilizer unit (flow rate 1 GPM; power 6 W; voltage 220 V) with the irradiation intensity of 0.3645mW/cm^2. A 20 ml sample was taken every 30 minutes and injected using a 0.2µm PVDF syringe filter. UV-vis Spectrophotometer was used to investigate the concentration of contaminant.

3. Results and Discussion

3.1. Characterization of materials

The surface characteristics of the prepared samples, as

visualized in Fig. 1, were examined using Scanning electron microscopy (SEM). The SEM analysis of BSP samples confirmed the successful immobilization of TiO_2 on the external surface of the biochar by the sol-gel method. TiO_2 nanocrystals were deposited on the biochar surface through reactions [31]:

Hydrolysis

$$\equiv Ti - O - R + H_2O \rightarrow \equiv Ti - O - H + R - O - H \quad (1)$$

Condensation (Dehydration)

$$\equiv Ti - O - H + \equiv Ti - O - H \rightarrow \equiv Ti - O - Ti \equiv + H_2O \quad (2)$$

Condensation (Dealcoholation)

$$\equiv Ti - O - R + \equiv Ti - O - H \rightarrow \equiv Ti - O - Ti \equiv + R - O - H \quad (3)$$

Alcohol Exchange

$$\equiv Ti - O - R + R' - O - H \rightarrow \equiv Ti - O - R' + R - O - H \quad (4)$$

Calcination

$$\equiv Ti - O - R \rightarrow O = Ti = O + H_2O + CO_2 \quad (5)$$

All BSP composites synthesized with various volumes of TTIP demonstrated discernible TiO_2 aggregation on the biochar surface. The SEM analysis revealed that increasing the TTIP-to-biochar volume ratio led to a corresponding increase in particle size, likely due to the enhanced aggregation of TiO_2 nanoparticles during the precipitation stage of the synthesis process as described in a prior study by Fazal et al. [32]. TiO_2 loading became a key factor affecting the adsorption efficiency of the composite as it altered its specific surface area, pore structure, and porosity [33].

In particular, the BSP-25 sample, synthesized with the highest TiO_2 loading, displayed significantly altered surface characteristics, including a notable reduction in pore volume and surface porosity compared to BSP-15 and BSP-20. These morphological changes are consistent with the observed adsorption performance, wherein BSP-25 exhibited a reduced degradation rate under dark conditions. This observation is aligned with findings reported in previous studies by Thuan et al. [34] and Liu et al. [35]. This diminished activity is likely attributable to the extensive TiO_2 agglomeration, which may have impeded access to the active adsorption sites on the biochar surface [36], thereby limiting its effectiveness.

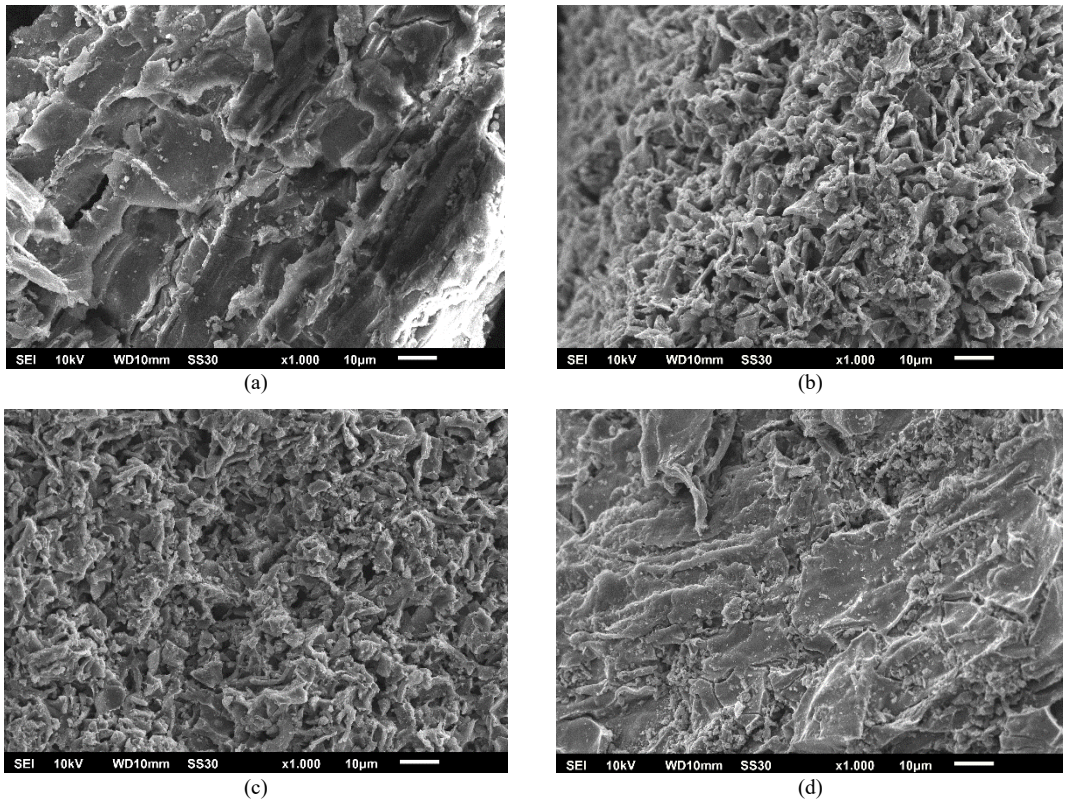

Fig. 1. SEM image of (a) Biochar; (b) BSP 15; (c) BSP 20; (d) BSP 25

FTIR spectrum, as shown in Fig. 2, had a similar pattern for biochar and BSP. The wavenumber explained that the characteristic peaks in the range of 2885 to 3390 cm^{-1} from all the analyzed materials showed different surfaces on −OH groups, which were derived from cellulose, hemicellulose, and lignin contained in mangrove plants. The decline observed in –OH band intensity was determined by multiple factors, notably the thermal decomposition of hemicellulose, which began to undergo hydrolysis at approximately 200°C [37], or the engaged biochar in a bond-breaking interaction with TiO_2 [38, 39]. Thus, the incorporation of TiO_2 led to a reduction in the amount of surface hydroxyl groups.

All samples exhibited similar adsorption peak in the range of 1590 to 1616 cm^{-1}, describing the existence of C=C and C=O aromatic rings [40]. Additionally, the $-CH_2$ deformation vibration and C−O stretching vibration indicated that the biochar surface contained a wide variety of functional groups. The adsorption peak corresponding to O−O bond vibration observed in the range of 440 to 576 cm^{-1} indicated the formation of peroxyl bonds on the biochar surface following the TiO_2 loading [41]. As widely reported for TiO_2, the band observed in all BSP samples at wavenumbers around 500 cm^{-1}

is generally associated to Ti−O−Ti and/or Ti−O stretching vibrations [42]. This indicated that TiO_2 was successfully synthesized on the surface of Mangrove Biochar.

Table 1 presents the summary of the details of the functional group of the mangrove biochar and all BSP samples.

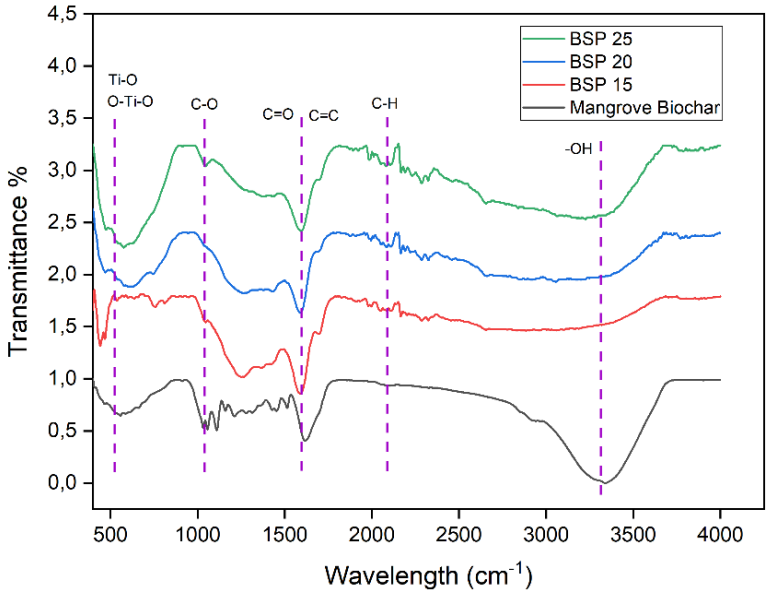

Fig. 2. FTIR spectra of biochar and BSP

Table 1. Functional group of biochar (BC) and BSP

Wavenumber (cm^{-1})				Annotation
BC	BSP 15	BSP 20	BSP 25	
-	440.87	492.04	476.74	O-Ti-O and Ti-O stretching vibration
557.39	-	-	-	C-H bending from aromatic ring
1032.44	-	-	-	(C-O) stretching vibrations ester and aliphatic ether
1427.44	1218.33	1234.31	1265.48	(C=O) stretching vibrations
1616.02	1590.02	1589.07	1593.32	(C=C) and (C=O) stretching and bending vibrations
2101.90	2213.67	2165.23	2183.97	(C-H) stretching aliphatic compounds (CH_3, CH_2)
3339.69	2984.25	3055.08	3225.85	(O-H) stretching vibrations

Fig. 3 depicts the XRD patterns of pristine TiO_2 and BSP composites with an output regarding the crystal structure phase of the TiO_2 material [43]. The presence of anatase-phase TiO_2 was confirmed by diffraction peaks at 2θ values of approximately 25.4°, 38.3°, 48.1°, 53.9°, and 62.8°, which corresponded to the (101), (004), (200), (105), (211), and (204) crystal planes, referenced in JCPDS No. 21-1272 [44].

A progressive increase in peak intensity from BSP 15 to BSP 25 indicated a higher degree of TiO_2 crystallinity, as more TiO_2 was incorporated into the composite. The pronounced peak at approximately 25.3° confirmed the dominance of the anatase phase, which was widely recognized for its effective photocatalytic performance. This result suggested that rutile TiO_2 was present only in negligible amounts, as indicated by a weak peak observed near 54.5°. Zheng et al. [45] reported that photocatalysts featuring both anatase and rutile phases were more effective.

In addition, no obvious diffraction peaks associated with the biochar component were observed, likely due to its disordered, amorphous structure or the overshadowing effect caused by the crystalline TiO_2 signals [46]. This suggested that TiO_2 nanoparticles were well-distributed and successfully anchored on the biochar surface.

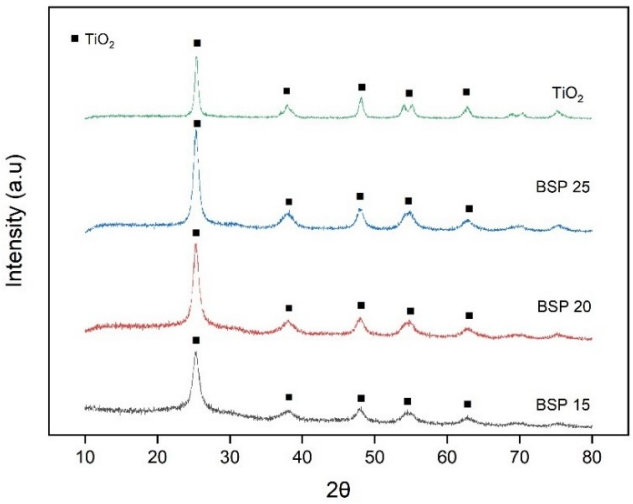

Fig. 3. XRD pattern of BSP

3.2. Adsorption and photocatalytic activity of BSP

The degradation performance of methylene blue in dark conditions indicated that biochar had more adsorption capacity than other materials. It had twice as much adsorption capability than BSPs. As the adsorption mechanism of materials is determined by their functional groups [47], the experiment results showed that mangrove biochar had the largest functional group area (Fig. 4), reaching 132.7939 m^2/g. It was conformable to its adsorption capability. The functional groups (hydroxyl, carboxyl, carbonyl, and amine) contained in biochar support the adsorption of organic molecules and enhance their affinity [48]. This adsorption pathway applies an electron donor/acceptor according to the irregular distribution of electrons among the functional group of the biochar and the organic material [49].

BSP 25 had the lowest adsorption capability of other samples. The functional group area of each BSP (Fig. 4) was 7.60198 m^2/g (BSP 15), 4.41947 m^2/g (BSP 20), and 4.39923 m^2/g (BSP 25). BSP proved a smaller functional group area compared to biochar because of the dispersion of TiO_2 into the spongy structure of Biochar [50]. BSP 15 also had a different Ti-O peak at 440 to 576 cm-1 than other BSP but its functional group area was larger than that of BSP 20 and BSP 25. This might be due to the clumping of TiO_2 in the sample [51], which caused Ti-O in BSP 15 to be unequally distributed.

Based on the characterization results, the marked improvement in the degradation efficiency of organic pollutants in dyed wastewater by BSP can be primarily ascribed to the strong interfacial interaction between biochar (BC) and TiO_2 within the composite structure. Accordingly, a plausible mechanism underlying the photocatalytic adsorption and subsequent reduction of methylene blue (MB) under UV irradiation by BSP is proposed and illustrated in Fig. 5. The adsorption-photocatalytic mechanism of BSP occurs in stages: (i) biochar in the composite serves as an adsorbent for dye (MB). Therefore, a large quantity of MB is adsorbed onto the biochar. (ii) over light illumination, electron-hole pairs (e-/h+) are produced inside TiO_2 nanoparticles deposited on biochar that break the MB adsorbed on the surface of biochar.

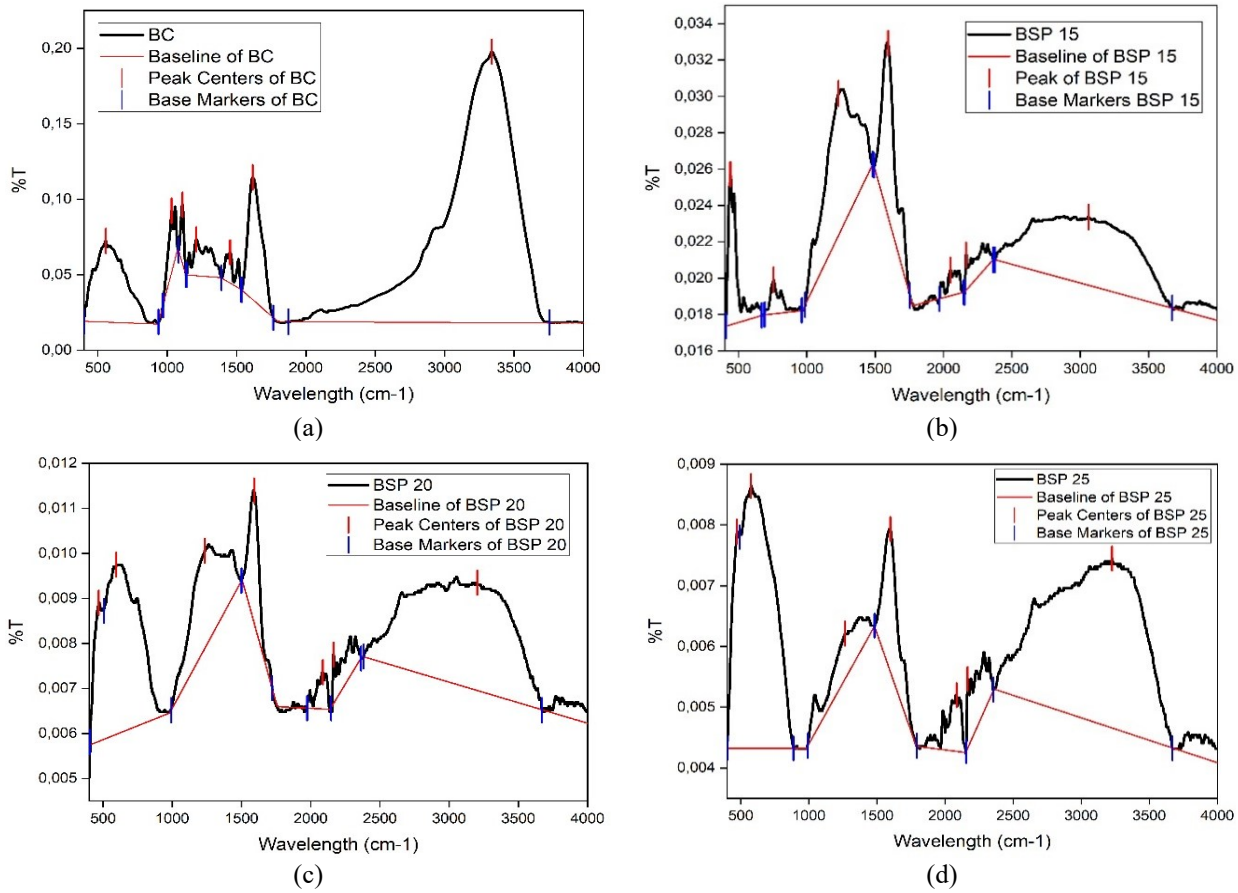

Fig. 4. Functional group area of (a) biochar and (b,c,d) BSPs

As illustrated in the proposed mechanism (Fig. 5), biochar serves as a porous carbonaceous support that enhances the surface area and provides abundant active sites [36] for the initial adsorption of MB molecules from solution. Under the UV irradiation, TiO_2 absorbs energy that excites electrons (e^-) in the valence band (VB) into the conduction band (CB), resulting in the formation of positive holes (h^+) in the VB. The photogenerated electrons are capable of reducing oxygen (O_2) molecules to reactive oxygen species (ROS), such as superoxide radicals ($•O_2^-$), while the holes can oxidize adsorbed MB or water molecules to form hydroxyl radicals (•OH), both of which are powerful oxidants that contribute to the breakdown of MB.

The absorbance obtained from UV-Vis analysis explained that the concentration of the MB dye solution significantly decreased when being degraded using BSP under UV

irradiation conducted in 3 times replication. The BSP-20 with a catalyst loading of 0.5 g/L exhibited an impressive degradation capability on 100% MB dye removal within 150 minutes of UV irradiation.

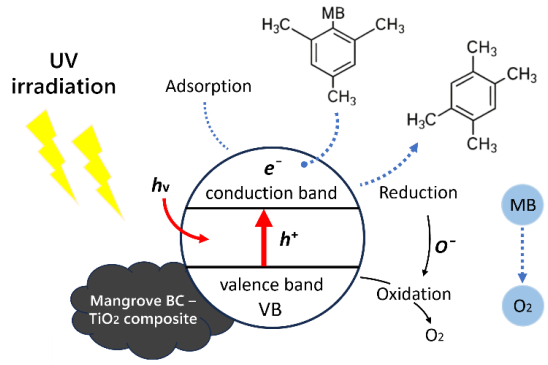

Fig. 5. Adsorption-photocatalytic mechanism of BSP in methylene blue

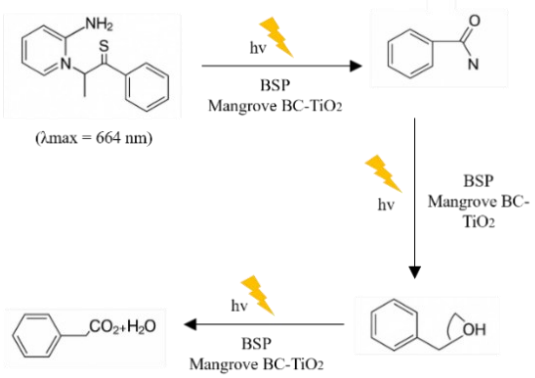

Fig. 6. Proposed pathway of degraded MB

UV–Vis spectrum analysis revealed a continuous decline in the absorption peak at ≈664 nm, indicating the progressive destruction of the chromophoric structure of methylene blue. The appearance of new absorbance features in the UV region (<300 nm) suggested the formation of lower molecular weight intermediates. Based on these observations and supported by previous studies, a proposed degradation pathway involving demethylation, ring cleavage, and eventual mineralization is suggested in Fig. 6.

The photodegradation kinetics of MB were described by a first-order model, indicating a concentration-dependent reaction rate [34,52]. The direct relationship existed between the reaction rate and the residual MB concentration in the solution (C), which is mathematically expressed as follows:

$$\ln \frac{C}{C_0} = k.t \qquad (6)$$

C is an organic concentration at a specific time, C_0 is the starting concentration, k is the kinetics reaction constant, and t is time. Different samples were loaded in MB solution and BSP 20 resulted in the highest degradation kinetic constant with k = 0.021/min. This result aligned with earlier findings by previous work by Guo et al. [20] that applied similar kinetic model to investigate the synergistic interaction between biochar and TiO_2 in a composite derived from rice husk biomass and Tetra n butyl titanate (TNBT). In their study, the BC-TiO_2 composite achieved a kinetic rate constant of 3.15×10^{-3} min^{-1} for the toluene degradation via a combined adsorption–photocatalysis mechanism. The comparison highlighted the enhanced photocatalytic performance of BSP 20, likely attributed to improved interfacial contact and surface functionality within the composite system.

The degradation curves and kinetic constants of MB at various catalysts are presented in Fig. 7 and Fig. 8, respectively. The photocatalysis phenomenon is a multiple process reinforced by several process parameters such as temperature, light intensity, pH, concentration of pollutant, and catalyst dosage. In typical experiments, The degradation rate rises as the catalyst loading in the system increases [53] because adding a catalyst enhances the number of -OH radicals produced. In addition, the surface area available increases for higher adsorption-degradation capabilities. Nonetheless, there is a preferred catalyst concentration level for achieving photocatalysis under UV light. This study observed that the opacity may increase above its limit, thereby reducing light penetration through the environment due to increased light scattering from catalyst particles [54]. However, the following equation assesses the efficiency (η) of the concentrations in the photocatalytic solution.

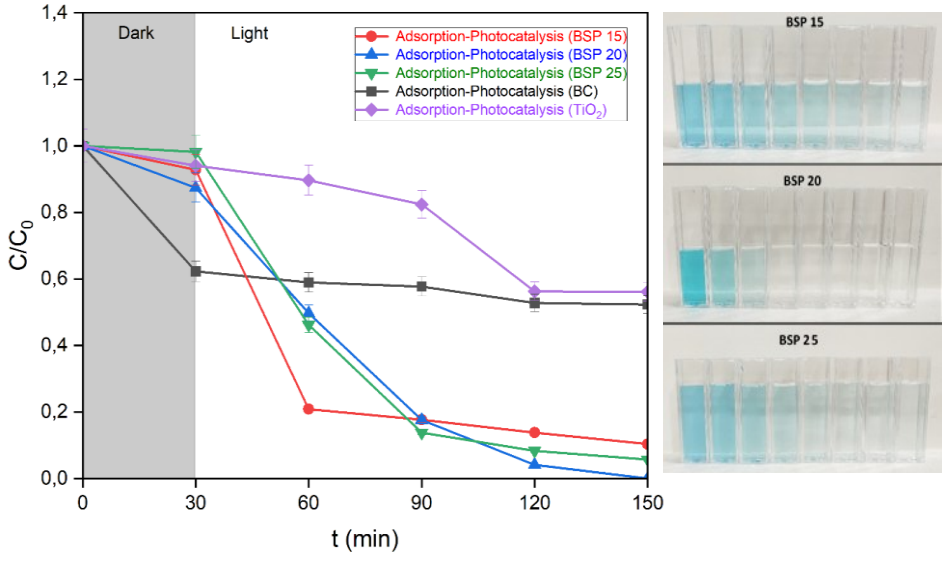

Fig. 7. Reduction of MB concentration in adsorption-photocatalysis process using BSP, adsorption using BC, and photocatalysis using TiO_2

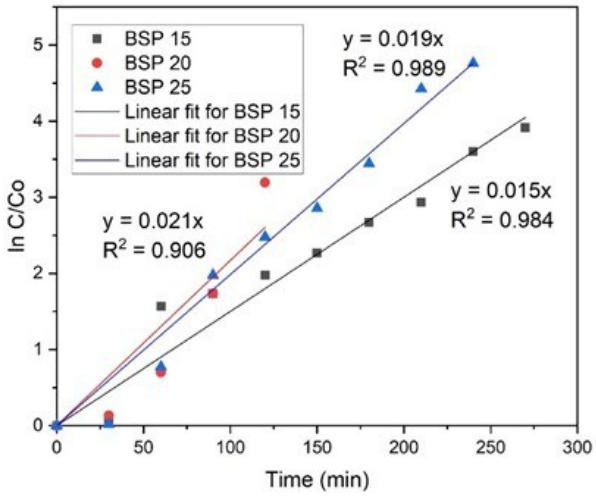

Fig. 8. Photodegradation profiles and kinetic constant of MB

$$\eta = 1 - \left(\frac{C}{C_0}\right) \times 100\% \quad (7)$$

where C_0 and C represent the concentrations of solutions before and after exposure [55]. The highest efficiency rate of photocatalytic obtained by BSP 20 was able to degrade 100% of MB solution with a catalyst dosage of 0.5 g/L.

The results obtained in this research are consistent with prior findings by Du et al. [56], reporting that a TiO_2–biochar composite synthesized from agricultural biomass and TNBT effectively degraded Cr(VI) with a 99.9% removal rate under UV exposure within 25 minutes. This result further supports the corroboration of synergistic interaction in biochar-supported photocatalysts and emphasizes the potential of the BSP composite for application in dyed wastewater treatment.

4. Conclusion

The BSP composites demonstrated strong potential for the removal of methylene blue (MB), achieving over 99% efficiency, clearly outperforming both unmodified biochar and pure TiO_2. This observed improvement was ascribed to the synergistic interaction between biochar and TiO_2. While the incorporation of TiO_2 led to a reduction in the surface functional groups of biochar, it substantially improved its photodegradation capability under UV light. The kinetic data reinforced the presence of this synergistic effect, as the BSP composites exhibited a significantly higher degradation rate compared to other samples. Notably, the BSP-20 sample achieved complete MB removal after 30 minutes of dark adsorption followed by 120 minutes of UV-driven photocatalysis at a dosage of 0.5 g/L.

These findings underline the critical role of catalyst dosage in determining solution concentration and light penetration, thereby impacting overall photocatalytic efficiency. Given its high removal efficiency, the BSP composite emerges as a promising candidate for the treatment of dye-contaminated wastewater. It is worth highlighting that further research should consider optimizing degradation efficiency under various environmental conditions with a systematic investigation into a number of key parameters such as pH, light intensity, and irradiation duration.

Acknowledgments

The authors acknowledged the Directorate General of Higher Education, Research and Technology, Ministry of Education, Culture, Research and Technology, Indonesia, for the financial support No: 449A-74/UN7.D2/PP/VI/2023 as well as Diponegoro University World Class University Program 2024

References

1. World Wildlife Foundation, *Water Scarcity*, (2023). https://www.worldwildlife.org/threats/water-scarcity.
2. B. Pratap, S. Kumar, S. Nand, I. Azad, R.N. Bharagava, L.F. Romanholo Ferreira, V. Dutta, *Wastewater generation and treatment by various eco-friendly technologies: Possible health hazards and further reuse for environmental safety*, Chemosphere 313 (2023) 137547.
3. R. Al-Tohamy, S.S. Ali, F. Li, K.M. Okasha, Y.A.G. Mahmoud, T. Elsamahy, H. Jiao, Y. Fu, J. Sun, *A critical review on the treatment of dye-containing wastewater: Ecotoxicological and health concerns of textile dyes and possible remediation approaches for environmental safety*, Ecotoxicol. Environ. Saf. 231 (2022) 113160.
4. A.P. Periyasamy, *Textile Dyes in Wastewater and its Impact on Human and Environment: Focus on Bioremediation*, Water, Air, Soil Pollut. 236 (2025) 562.
5. E. Weidner, E. Karbassiyazdi, A. Altaee, T. Jesionowski, F. Ciesielczyk, *Hybrid Metal Oxide / Biochar Materials for Wastewater Treatment Technology : A Review*, (2022).
6. S. Kathi, A. El Din Mahmoud, *Trends in effective removal of emerging contaminants from wastewater: A comprehensive review*, Desalin. Water Treat. 317 (2024) 100258.
7. F. Amalina, A. Syukor, A. Razak, S. Krishnan, H. Sulaiman, A.W. Zularisam, M. Nasrullah, *Journal of Hazardous Materials Advances Biochar production techniques utilizing biomass waste-derived materials and environmental applications – A review*, J. Hazard. Mater. Adv. 7 (2022) 100134.
8. I. Ben Salem, M. El Gamal, M. Sharma, S. Hameedi, F.M. Howari, *Utilization of the UAE date palm leaf biochar in carbon dioxide capture and sequestration processes*, J. Environ. Manage. 299 (2021) 113644.
9. X. Wang, Y. Li, H. Wang, Y. Wang, A. Biswas, H. Wai Chau, J. Liang, F. Zhang, Y. Bai, S. Wu, J. Chen, H. Liu, G. Yang, A. Pulatov, *Targeted biochar application alters physical, chemical, hydrological and thermal properties of salt-affected soils under cotton-sugarbeet intercropping*, Catena 216 (2022).
10. R.K. Mishra, K. Mohanty, *A review of the next-generation biochar production from waste biomass for material applications*, Sci. Total Environ. 904 (2023) 167171.
11. E. Cárdenas-Aguiar, G. Gascó, M. Lado, A. Méndez, J. Paz-Ferreiro, A. Paz-González, *Characterization of Biochar from Beach-Cast Seaweed and Its Use for Amelioration of Acid Soils*, Land 13 (2024).
12. K. Liu, A. Zhang, X. Liu, T. Liang, X. Li, K. Hu, F. Ji, H. Li, X. Chen, X. Fu, *N,S-codoped carbon microporous structures derived from dead ginkgo leaves as efficient oxygen reduction reaction catalysts for Al-air batteries*, New J. Chem. 48 (2024) 12423–12433.
13. M. Naderi, M. Vesali-Naseh, *Hydrochar-derived fuels from waste walnut shell through hydrothermal carbonization: characterization and effect of processing parameters*, Biomass Convers. Biorefinery 11 (2021) 1443–1451.
14. M. Omenesa, M. Nasir, M. Ibrahim, N. Asshifa, A. Ali, M.H. Hussin, *Synthesis and fabrication of palm kernel shell-derived modified*

electrodes : A practical step towards the industrialization of microbial fuel cells, Chem. Eng. J. 475 (2023) 146321.

15. W.R. Khan, M.O. Aljahdali, *Elemental Composition of Above and Belowground Mangrove Tissue and Sediment in Managed and Unmanaged Compartments of the Matang Mangrove Forest Reserve*, Plants 11 (2022).
16. R. Ray, T.K. Jana, *Carbon sequestration by mangrove forest: One approach for managing carbon dioxide emission from coal-based power plant*, Atmos. Environ. 171 (2017) 149–154.
17. H. Thi, C. Marchand, J. Aimé, D. Hoai, P. Nguyen, N. Xuan, N. Thi, K. Cuc, *Belowground carbon sequestration in a mature planted mangroves (Northern Viet Nam)*, For. Ecol. Manage. 407 (2018) 191–199.
18. I. Sulthonuddin, H. Herdiansyah, *Sustainability of Batik wastewater quality management strategies: analytical hierarchy process*, Appl. Water Sci. 11 (2021) 1–12.
19. W. Wang, D. Li, S. Zuo, Z. Guan, H. Xu, S. Ding, D. Xia, *Colloids and Surfaces A : Physicochemical and Engineering Aspects Discarded-leaves derived biochar for highly efficient solar water evaporation and clean water production : The crucial roles of graphitized carbon*, Colloids Surfaces A Physicochem. Eng. Asp. 639 (2022) 128337.
20. D. Guo, D. Feng, Y. Zhang, Z. Zhang, J. Wu, Y. Zhao, *Synergistic mechanism of biochar-nano TiO 2 adsorption-photocatalytic oxidation of toluene*, Fuel Process. Technol. 229 (2022) 107200.
21. M.A. Martins, M. Otero, C. Patrícia, D. Pereira, V.I. Esteves, D.L.D. Lima, *Biochar-TiO 2 magnetic nanocomposites for photocatalytic solar-driven removal of antibiotics from aquaculture effluents*, 294 (2021).
22. M. Ulfa, I.U. Hasanah, H. Bahruji, *Understanding the regenerating capacity on photodegradation of methylene blue of titania supported mesoporous silica with the aid of gelatin-P123 as bitemplate*, Commun. Sci. Technol. 9 (2024) 282–290.
23. Z. Liu, A. Quek, S. Kent Hoekman, R. Balasubramanian, *Production of solid biochar fuel from waste biomass by hydrothermal carbonization*, Fuel 103 (2013) 943–949.
24. E. Miliotti, D. Casini, L. Rosi, G. Lotti, A.M. Rizzo, D. Chiaramonti, *Lab-scale pyrolysis and hydrothermal carbonization of biomass digestate: Characterization of solid products and compliance with biochar standards*, Biomass and Bioenergy 139 (2020) 105593.
25. Z. Zhang, Z. Zhu, B. Shen, L. Liu, *Insights into biochar and hydrochar production and applications: A review*, Energy 171 (2019) 581–598.
26. Y. Yue, X. Yue, X. Tang, L. Han, J. Wang, S. Wang, C. Du, *Synergistic adsorption and photocatalysis study of TiO2 and activated carbon composite*, Heliyon 10 (2024) e30817.
27. J. Shi, W. Huang, H. Zhu, J. Xiong, H. Bei, S. Wang, *Facile Fabrication of Durable Biochar / H 2 - TiO 2 for Highly E ffi cient Solar-Driven Degradation of Enro fl oxacin : Properties , Degradation Pathways , and Mechanism*, (2022).
28. X. Zhang, L. Zhang, A. Li, *Eucalyptus sawdust derived biochar generated by combining the hydrothermal carbonization and low concentration KOH modification for hexavalent chromium removal*, J. Environ. Manage. 206 (2018) 989–998.
29. M.M. Mian, G. Liu, *Recent progress in biochar-supported photocatalysts: Synthesis, role of biochar, and applications*, RSC Adv. 8 (2018) 14237–14248.
30. S. Chandra, P. Jagdale, I. Medha, A.K. Tiwari, M. Bartoli, A. De Nino, F. Olivito, *Biochar-supported tio2-based nanocomposites for the photocatalytic degradation of sulfamethoxazole in water—a review*, Toxics 9 (2021).
31. S. Zhang, X. Lu, *Treatment of wastewater containing Reactive Brilliant Blue KN-R using TiO2/BC composite as heterogeneous photocatalyst and adsorbent*, Chemosphere 206 (2018) 777–783.
32. T. Fazal, A. Razzaq, F. Javed, A. Hafeez, N. Rashid, U.S. Amjad, M.S. Ur Rehman, A. Faisal, F. Rehman, *Integrating adsorption and photocatalysis: A cost effective strategy for textile wastewater treatment using hybrid biochar-TiO2 composite*, J. Hazard. Mater. 390 (2020) 121623.
33. S. Silvestri, N. Stefanello, A.A. Sulkovski, E.L. Foletto, *Preparation of TiO2 supported on MDF biochar for simultaneous removal of methylene blue by adsorption and photocatalysis*, J. Chem. Technol. Biotechnol. 95 (2020) 2723–2729.
34. D. Van Thuan, T.T.H. Chu, H.D.T. Thanh, M.V. Le, H.L. Ngo, C.L. Le, H.P. Thi, *Adsorption and photodegradation of micropollutant in wastewater by photocatalyst TiO2/rice husk biochar*, Environ. Res. 236 (2023) 116789.
35. W. Liu, B. Wang, M. Zhang, *Effect of Process Parameters on the Microstructure and Performance of TiO2-Loaded Activated Carbon*, ACS Omega 6 (2021) 35076–35092.
36. Y. Liu, X. Dai, J. Li, S. Cheng, J. Zhang, Y. Ma, *Recent progress in TiO2-biochar-based photocatalysts for water contaminants treatment: strategies to improve photocatalytic performance*, RSC Adv. 14 (2024) 478–491.
37. D.I. Lestari, A.T. Yuliansyah, A. Budiman, *Adsorption studies of KOH-modified hydrochar derived from sugarcane bagasse for dye removal: Kinetic, isotherm, and thermodynamic study*, Commun. Sci. Technol. 7 (2022) 15–22.
38. J. Wang, Y. Chen, *RSC Advances*, (2023) 24237–24249.
39. H. Hosseini-Monfared, Y. Mohammadi, R. Montazeri, S. Gasemzadeh, R.S. Varma, *Effect of biochar on the photocatalytic activity of nitrogen-doped titanium dioxide nanocomposite in the removal of aqueous organic pollutants under visible light illumination*, Nanochemistry Res. 6 (2021) 79–93.
40. S. Pasieczna-Patkowska, M. Cichy, J. Flieger, *Application of Fourier Transform Infrared (FTIR) Spectroscopy in Characterization of Green Synthesized Nanoparticles*, Molecules 30 (2025) 1–36.
41. A.M. Abodif, L. Meng, S. Ma, A.S.A. Ahmed, N. Belvett, Z.Z. Wei, *Mechanisms and Models of Adsorption : TiO 2 - Supported Biochar for Removal of 3 , 4-Dimethylaniline*, (2020).
42. M. Karamifar, S. Sabbaghi, M.S. Mohtaram, K. Rasouli, M. Mohsenzadeh, H. Kamyab, A. Derakhshandeh, L. Dolatshah, H. Moradi, S. Chelliapan, *Ultrasonic-assisted synthesis of TiO2/MWCNT/Pani nanocomposite: Photocatalyst characterization and optimization of efficient variables in the degradation of benzene via RSM-CCD*, Powder Technol. 432 (2024) 119176.
43. D. Castilla-Caballero, A. Hernandez-Ramirez, S. Vazquez-Rodriguez, J. Colina-Márquez, F. Machuca-Martínez, J. Barraza-Burgos, A. Roa-Espinosa, A. Medina-Guerrero, S. Gunasekaran, *Effect of pyrolysis, impregnation, and calcination conditions on the physicochemical properties of TiO2/Biochar composites intended for photocatalytic applications*, J. Environ. Chem. Eng. 11 (2023).
44. F. Scarpelli, T.F. Mastropietro, T. Poerio, N. Godbert, *Mesoporous TiO2 Thin Films: State of the Art*, Titan. Dioxide - Mater. a Sustain. Environ. (2018).
45. J. Zheng, J. Cai, S. Li, R. Li, M. Huang, *Regulation of a rutile/anatase TiO2 heterophase junction in situ grown on Ti3C2Tx MXenes with remarkable photocatalytic properties*, New J. Chem. 48 (2024) 15830–15838.
46. M. Abdu, A. Worku, S. Babaee, P. Diale, T.A. Msagati, J.F. Nure, *The development of TiO2-biochar composite material for photodegradation of basic blue 41 and erichrome black T azo dyes from water*, Surfaces and Interfaces 62 (2025) 106156.
47. K. Yadav, S. Jagadevan, *Influence of torrefaction and pyrolysis on engineered biochar and its applicability in defluoridation: Insight into adsorption mechanism, batch adsorber design and artificial neural network modelling*, J. Anal. Appl. Pyrolysis 154 (2021) 105015.

48. X. Dong, Y. Chu, Z. Tong, M. Sun, D. Meng, X. Yi, *Ecotoxicology and Environmental Safety Mechanisms of adsorption and functionalization of biochar for pesticides : A review*, Ecotoxicol. Environ. Saf. 272 (2024) 116019.
49. A. Fakhar, S.J.C. Galgo, R.C. Canatoy, M. Rafique, R. Sarfraz, A.A. Farooque, M.I. Khan, *Advancing modified biochar for sustainable agriculture: a comprehensive review on characterization, analysis, and soil performance*, Biochar 7 (2025).
50. A.M. Abodif, A.M. Abodif, L. Meng, S. Ma, A.S.A. Ahmed, N. Belvett, Z.Z. Wei, D. Ning, *Mechanisms and Models of Adsorption: TiO2-Supported Biochar for Removal of 3,4-Dimethylaniline*, ACS Omega 5 (2020) 13630–13640.
51. X. Shu, X. Liu, *Efficacy and mechanism of nano-biochar supported TiO2 in removing dichloroacetic acid from swimming pools*, Rev. Mater. 29 (2024).
52. F. Riyanti, H. Hasanudin, A. Rachmat, W. Purwaningrum, P.L. Hariani, *Photocatalytic degradation of methylene blue and Congo red dyes from aqueous solutions by bentonite-Fe3O4 magnetic*, Commun. Sci. Technol. 8 (2023) 1–9.
53. M. Gar, A. Taw, S. Ookawara, *Journal of Environmental Chemical Engineering Enhancement of photocatalytic activity of TiO 2 by immobilization on activated carbon for degradation of pharmaceuticals*, 4 (2016) 1929–1937.
54. D. Ariyanti, M. Maillot, W. Gao, *Journal of Environmental Chemical Engineering Photo-assisted degradation of dyes in a binary system using TiO 2 under simulated solar radiation*, J. Environ. Chem. Eng. 6 (2018) 539–548.
55. S. Alomairy, L. Gnanasekaran, S. Rajendran, W.F. Alsanie, *Biochar supported nano core-shell (TiO2/CoFe2O4) for wastewater treatment*, Environ. Res. 238 (2023) 117169.
56. Y. Du, X. Ye, Z. Hui, D. Jiao, Y. Xie, S. Chen, J. Ding, *Synergistic effect of adsorption-photocatalytic reduction of Cr(vi) in wastewater with biochar/TiO2 composite under simulated sunlight illumination*, Phys. Chem. Chem. Phys. 26 (2024) 15891–15901.